Significant decrease of the optical losses in the coupling between colloidal CdSe/CdS nanocrystals and a flat gold film at cryogenic temperature

A. Coste,[1] F. Eloi,[1] C. Arnold,[1] G. Colas des Francs,[2] X. Quélin,[1] S. Buil,[1] A. Bouhelier,[2] J. C. Weeber,[2] M. Nasilowski,[3] B. Dubertret,[3] and J.-P. Hermier[1,*]

[1]*Groupe d'Etude de la Matière Condensée (GEMaC), Université de Versailles Saint-Quentin-en-Yvelines, CNRS UMR 8635, Université Paris-Saclay, 45 Avenue des Etats-Unis, 78035 Versailles Cedex, France*

[2]*Laboratoire Interdisciplinaire Carnot de Bourgogne (ICB), UMR 6303 CNRS, Université Bourgogne Franche-Comté, 9 Avenue Savary, BP 47870, 21078 Dijon Cedex, France*

[3]*Laboratoire de Physique et d'Étude des Matériaux, CNRS UMR8213, ESPCI, 10 Rue Vauquelin, 75231 Paris, France*

(Received 20 July 2017; revised manuscript received 5 September 2017; published 9 November 2017)

We investigate the influence of the temperature (between 4 K and room temperature) on the fluorescence of colloidal thick-shell CdSe/CdS nanocrystals coupled with a flat gold film. First, we deduce the complex dielectric function ϵ from the spectrophotometric measurements on the flat gold film. Then, when compared to a nanocrystal deposited on a glass coverslip, calculations show that the enhancement of the photoluminescence decay rate is divided by a factor of 2.3 between 11 and 293 K due to the reduction of optical losses. Our analysis well accounts for the experiments performed on single CdSe/CdS nanocrystals.

DOI: 10.1103/PhysRevB.96.195416

I. INTRODUCTION

Metallic structures have attracted great attention since they are very promising for applications such as spectroscopy [1], light harvesting in photovoltaic devices [2], optical sensors measuring the concentration of chemicals [3], and optical devices for biology [4] or nanomedicine [5]. In the field of nanophotonics, the use of plasmonic nanostructures represents a relevant approach to enhance the fluorescence of nanoemitters and to collect it efficiently [6–9]. Indeed, in contrast with dielectric structures, plasmonic ones offer the possibility to achieve subdiffraction confinement of light and to manipulate the electromagnetic field at the nanoscale [10]. However, metals that are commonly used such as silver or gold exhibit high optical losses, especially at visible wavelengths [11–13]. For practical applications, techniques to remedy this drawback are then in high demand.

The imaginary part of the dielectric permittivity of metal quantifies the optical losses. It is also proportional to the electron ohmic resistivity. Joule and optical losses are then closely linked. Recently, the reduction of ohmic losses was investigated in flat silver films [14,15]. The crucial role of the film crystallinity and the surface roughness has been highlighted. Beyond these structural effects, electron-phonon scattering ultimately limits the plasmon damping. It can be reduced with low-temperature operation. In the case of a flat silver film, the plasmon propagation length at the film interface can be enhanced by a factor of 1.5 when decreasing the temperature from 293 to 4 K. For an ensemble or individual gold bipyramid nanoparticles free of surface roughness, Liu *et al.* also reported a decrease of 30% of the homogeneous plasmon resonance linewidth [16].

In this paper, the effects of low-temperature operation on the optical properties of a gold film are first investigated. For temperature ranging between 11 and 293 K, the complex dielectric function ϵ of a low-roughness film is determined from spectroscopic absorption measurements and from the fit of the experimental data by a Drude and two critical points (DCP) model. The imaginary part of ϵ that is at the root of the optical losses decreases by a factor of the order of 2.5 around $\lambda = 600$ nm. The opportunities offered by the dramatic decrease of the optical losses are next illustrated through the coupling of colloidal nanocrystals (NCs) with the flat gold film. When compared to NCs deposited on glass, we predict and measure that the enhancement of the decay rate is 2.3 times lower at 11 K than at 293 K due to the reduction of the ohmic energy dissipation (the enhancement is equal to 15 at 293 K and 6.3 at 11 K). At the same time, the radiative quantum efficiency (QE) is 3.2 times greater.

II. EXPERIMENTS

A. Samples

The flat gold film was fabricated by thermal evaporation at room temperature of gold on a cleaned glass substrate under ultrahigh vacuum (10^{-9} Torr). The mass measured with a quartz balance shows that the continuous film has a thickness of 25 nm. Atomic force microscope measurements over a 1 μm $\times$ 1 μm area indicate that the roughness is equal to 1.1 nm.

The chemical synthesis of CdSe/CdS core-shell NCs is detailed in Ref. [17]. The core diameter measures 3 nm while the mean value of the shell thickness is 6 nm. The surface is encapsulated by ligands with a mean length of 2 nm. In the following, we consider that the shell and the ligands act as a spacer and that the NCs correspond to a degenerate dipole [18] located 10 nm above the surface they are deposited on. At room temperature, the emission wavelength is centered at 620 nm. At 4 K, it is about 590 nm.

B. Experimental setups

The NCs are suspended in a mixture of 90% hexane and 10% octane. They can be spin coated on a glass coverslip or a flat gold film so that single NCs can be studied with a confocal microscope setup operating between 4 and 293 K

*jean-pierre.hermier@uvsq.fr

(Cryostat attoDRY1100, low-temperature confocal microscope attoCFM I, attocube) without any drift for several hours. The NCs are optically excited by a pulsed laser diode (LDH D-C-485, Picoquant, wavelength operation of 485 nm, pulse duration ∼100 ps). The NC emission is collected with a 0.82 numerical aperture objective and detected by a Hanbury-Brown and Twiss setup (MPD avalanche photodiodes, time resolution of 50 ps) connected to a data-acquisition card (PicoHarp 300 module, Picoquant, 64 ps time resolution). The instrumental function response (IRF) of the overall setup was determined experimentally and is of the order of 200 ps.

The transmission measurements were driven with a spectrophotometer (Perkin Elmer LAMBDA 850) extended with a cryostat (CCS-400H-204, Janis), so that the sample temperature can be adjusted between 11 and 800 K. The absorption spectrum was measured between 11 and 293 K for wavelengths ranging from 400 to 800 nm.

III. RESULTS AND DISCUSSIONS

A. Gold-film dielectric constant and decay rate

The dielectric function ϵ of gold is tabulated in several data tables such as the ones of Johnson and Christy [19] or in Ref. [20]. However, when considering a thin gold film, one has to take into account its thickness and roughness. More fundamentally, ϵ also depends on the temperature and very few data on the optical properties of gold nanostructures were reported for cryogenic temperatures [16,21].

In order to characterize the studied gold film, the dielectric constant was determined by fitting the measured transmission coefficient of a glass/gold/air slab as a function of the wavelength. The glass dielectric constant is taken from tabulated data, assuming a Cauchy wavelength dependency. The gold dielectric constant is assumed to follow a DCP model in order to describe the metal optical response near the interband transitions [22] [see Eq. (1)]:

$$\epsilon(\omega) = \epsilon_\infty - \frac{\omega_p^2}{\omega^2 + i\omega\gamma_p} + \sum_{i=1}^{2} \frac{A_i\omega_i e^{i\phi_i}}{\omega_i - \omega - i\gamma_i} + \frac{A_i\omega_i e^{-i\phi_i}}{\omega_i - \omega + i\gamma_i}. \quad (1)$$

The two first terms refer to the Drude-like contribution with ϵ_∞ the high-frequency limit of the dielectric constant and γ_p the damping rate. The sum describes the interband transition with two critical point transitions at energies $\hbar\omega_{1,2}$, with a broadening $\gamma_{1,2}$ and a weight $A_{1,2}$. $\phi_{1,2}$ is the phase of the pole describing the interband transition. For the null phase, the critical point transition behaves like a Lorentz oscillator. The inclusion of a phase factor takes into account direct and indirect interband transitions within the Brillouin zone [23].

We present in Fig. 1 typical behaviors for two working temperatures (11 and 293 K). We consider the parameters fitted by Vial and Laroche for tabulated data at ambient temperature as the initial guess for our model [24]. The fitted parameters are presented as a function of the temperature in the Appendix. The main changes concern the loss rates. We notably observe a strong increase of the Drude loss rate γ_p and interband loss rates $\gamma_{1,2}$ near 125 K. The mean total Γ_{tot}

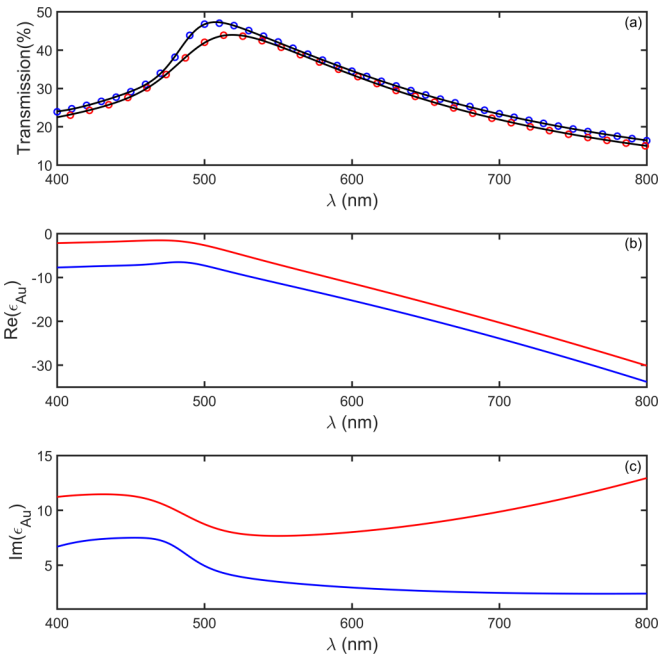

FIG. 1. (a) Transmission measured as a function of the wavelength for two temperatures: 11 K (blue circles) and 293 K (red circles). The experimental data are fitted using a Drude critical point model for the gold dielectric constant (black lines). (b) Real part of the gold-film dielectric constant estimated from the fits at 11 K (blue line) and 293 K (red line). (c) The same for the imaginary part.

and nonradiative Γ_{NR} decay rates of NCs above the gold film can be finally calculated using the Chance-Prock-Silbey model [25,26], as presented in Fig. 2 (the average is calculated for a distribution of NCs modeled as a two-dimensional dipole and presenting a random orientation). We observe a decrease of

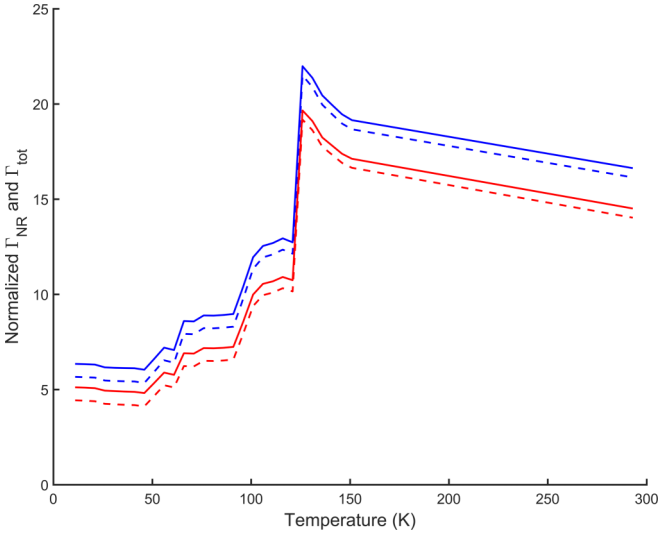

FIG. 2. Nonradiative (dashed lines) and total (continuous lines) decay rates as a function of temperature estimated considering the experimental gold dielectric constant of Figs. 1(b) and 1(c) (the values are normalized to the ones obtained for a glass coverslip). The emission wavelength is $\lambda_{em} = 590$ nm (blue) or 620 nm (red). The NC is 10 nm above the gold film.

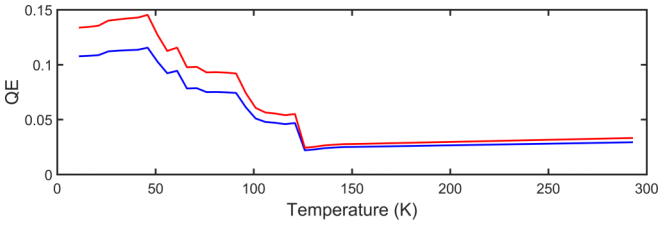

FIG. 3. QE as a function of the temperature. The emission wavelength is $\lambda_{em} = 590$ nm (blue) or 620 nm (red).

the normalized decay rates (the normalization is made with respect to the glass surface) at cryogenic temperatures, due to lower losses. Moreover, the decay rates are higher for smaller wavelengths, close to the gold interband transitions. In addition, the nonradiative rate strongly increases above 125 K, due to higher metal losses as revealed by the DCP model.

The relative contribution of Γ_{NR} with respect to Γ_{tot} also increases at 11 K. When the temperature increases, the gap between the nonradiative (dashed line) and total (continuous line) decay rates decreases; that is, the radiative rate decreases. Simultaneously the decay rates increase. As a consequence, the radiative QE also increases at cryogenic temperatures (Fig. 3). The total radiated power over 4π sr represents 3.3% of the total power at 293 K while it reaches 11% at 11 K.

B. Nanocrystal fluorescence

To illustrate the dramatic effect of the temperature on the coupling between a gold film and single NCs, we compare the results obtained at room temperature and the lowest temperature that can be reached with the cryostat (4 K). To start with, the emission of single NCs deposited on a glass coverslip is characterized at room temperature. In the following, we operate with low-power excitation such that the probability to generate one electron-hole pair per pulse is much higher than the probability to create several. Thick-shell CdSe/CdS NCs are then known to alternate between a bright state when the NC is neutral and a "grey" state when it is ionized. For the bright state, the radiative quantum efficiency is close to 1 and close to 40% for the grey one due to the competition between the radiative and the Auger recombinations for the trion. Adjusting the photoluminescence (PL) decay with a biexponential curve, we find that the mean lifetime of the exciton τ is 49 ns, in agreement with previous measurements [27] [see Fig. 4(a)].

To compare the results obtained when NCs are coupled to the flat gold film, we took care to keep the pumping rate constant. We then reduced the pumping power, taking into account the reflectivity of the film at 485 nm (41% at 293 K and 49% at 11 K according to the spectrophotometric measurements). Still at 293 K, the PL decay of NCs coupled to the flat gold film occurs much faster, as expected [Fig. 4(b)]. As previously reported [27,28], the PL decay also exhibits two components. The long component with a mean value of 3.4 ns still corresponds to the exciton recombination. The fast component, ~0.7 ns, corresponds to the trion deexcitation and to a large contribution of noise due to the low QE. The decay rate enhancement induced by the gold film is then equal to 14, a value very close to the one predicted in the previous section

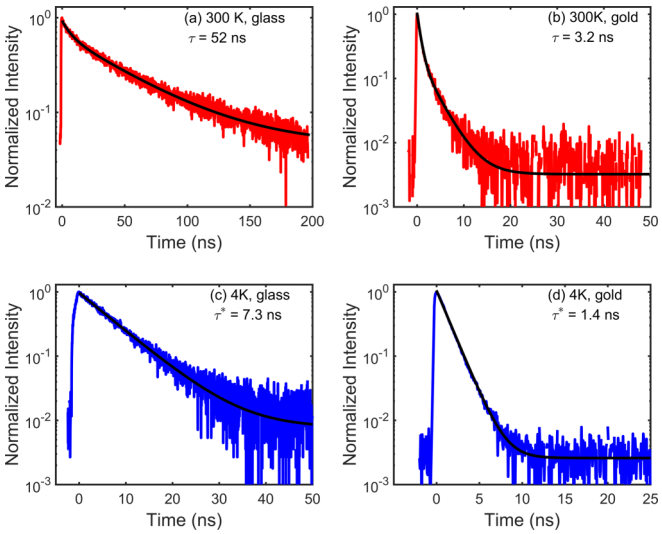

FIG. 4. (a) PL decay of a single NC deposited on glass at 293 K. The black line is a biexponential fit (lifetimes of 7 and 52 ns). (b) PL decay of a single NC deposited on the flat gold film at 293 K. The black line is a biexponential fit (lifetimes of 0.7 and 3.2 ns). (c) PL decay of a single NC deposited on glass at 4 K. The black line is a monoexponential fit (lifetime of 7.3 ns). (d) PL rate of a single NC deposited on the flat gold film at 4 K. The black line is a monoexponential fit (lifetime of 1.4 ns).

($\Gamma_{tot}/\Gamma_{glass} = 15$ at $\lambda = 620$ nm and room temperature; see Fig. 2).

The modification of the PL decay rate enhancement at 4 K is now investigated. Under vacuum, the PL decay and intensity measurements demonstrate that the NC remains in the charged state [29]. Due to the absence of air and water, once the NC is ionized, its neutralization cannot happen. At cryogenic temperatures, another crucial modification concerns the strong reduction of Auger recombinations efficiency, leading, for the trion, to a QE close to 1 under 30 K [29]. The QE for the charged biexciton can also reach values as high as 60% [30], with high variation from one NC to another [31], and the recombination of this state can contribute to the total fluorescence.

At 4 K, the PL decay of NCs on glass is then well fitted by a monoexponential decay or a biexponential decay depending on the potential contribution of the biexcitonic emission. The mean trion lifetime τ^* is 8.1 ns [7.3 ns for the data plotted in Fig. 4(c)]. For a few NCs, we also detected very long lifetime components (~20 ns, with a weight of 10%) that can be attributed to surface traps [32].

When NCs are coupled to the flat gold film at 4 K, the PL decay is well fitted by a monoexponential decay with very short lifetime [Fig. 4(d)]. The mean value is 1.6 ns so these measurements are not affected with the finite resolution of the experiment. Once again, for some NCs, we observed very long components (~5 ns) with small amplitudes (a few percent) corresponding to the formation of long-lived emission states.

From the two values of the trion lifetime measured at 4 K (8.1 ns on glass and 1.6 ns on gold), we calculate that the PL decay enhancement at this cryogenic temperature is equal to 5.1, a value close to the one predicted ($\Gamma_{tot}/\Gamma_{glass} = 6.3$ at

$\lambda = 590$ nm and 11 K; see Fig. 2). As already highlighted in Sec. III A, the decrease of the Purcell effect from 14 at 293 K to 5.1 at 4 K is due to the strong reduction of Joule losses and is associated to an enhancement of the overall radiative QE.

IV. CONCLUSION

In conclusion, the modification of the coupling between thick-shell CdSe/CdS NCs and a flat gold film at 4 K was investigated in detail. Measuring the variation of the flat film absorption spectrum with the temperature and fitting the spectra with a DCP model, we predict a dramatic reduction of the optical losses and an enhancement of the QE of the NCs. These results are in agreement with the experimental data obtained at the single-NC level.

Our results open new opportunities in terms of plasmonics applications. The reduction of the temperature in addition to the control of the film quality (surface defects, crystallinity of the metal) represents a relevant approach to reduce optical losses. The potential to enhance by a factor of 3 the radiative QE provides a strong motivation for future studies at cryogenic temperature, especially in the domain of quantum optics for which the reduction of the temperature also results in an improvement of the emitter optical properties (linewidth, QE). This strategy can also be extended to other nanoscale emitters.

ACKNOWLEDGMENTS

This work is supported by a public grant overseen by the French National Research Agency (ANR) as part of the "Investissements d'Avenir" program (Labex NanoSaclay, Grant No. ANR-10-LABX-0035). It is also supported by the ANR grant QDOTICS (Grant No. ANR-12-BS10-0008). Calculations were performed using HPC resources from DSI-CCuB (Université de Bourgogne).

APPENDIX: TEMPERATURE DEPENDENCE

We represent in Figs. 5–7 the DCP parameters used to fit the gold dielectric constant as a function of temperature. Concerning the Drude contribution (Fig. 5), the plasma frequency $\omega_p = \sqrt{Ne^2/m^\star\epsilon_0}$ does not significantly vary over the temperature range. This originates from a small decrease of the carrier density N with temperature that is compensated by a decrease of the effective mass $m^\star$ [33].

The decay rate γ_p is divided by 10, freezing from ambient to cryogenic temperatures, with a strong modification close to 125 K. The Drude decay rate originates from electron-electron (γ_{ee}) and electron-phonon (γ_{ep}) scattering processes [21],

$$\gamma_p = \gamma_{ee} + \gamma_{ep}, \tag{A1}$$

$$\gamma_{ee} = \frac{\pi^3 \Gamma \Delta}{12\hbar E_F}\left[(k_B T)^2 + \left(\frac{\hbar\omega}{2\pi}\right)^2\right], \tag{A2}$$

$$\gamma_{ep} = \omega_0\left[\frac{2}{5} + \frac{4T^5}{T_D}\int_0^{T_D/T_0}\frac{z^4}{e^z - 1}dz\right], \tag{A3}$$

where T_D is the gold Debye temperature.

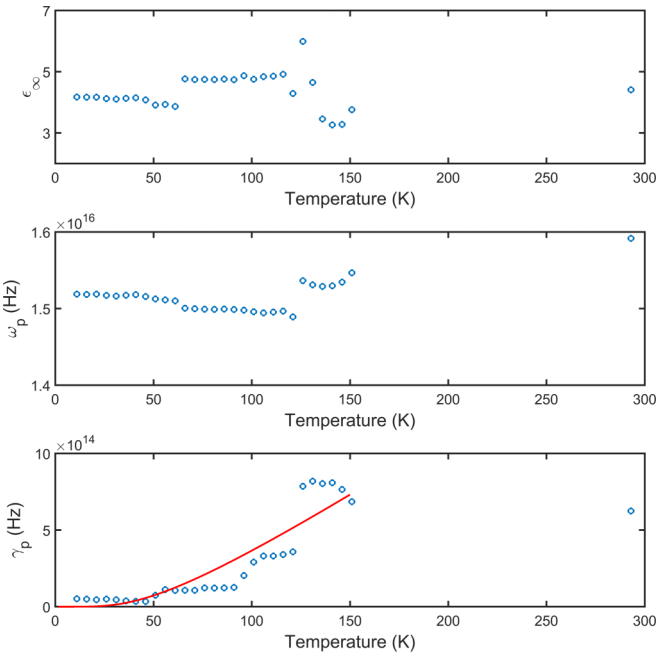

FIG. 5. Drude parameters ϵ_∞, ω_p, and γ_p as a function of the temperature.

Note that electron-electron scattering depends quadratically on both the temperature and the angular frequency (see γ_{ee} expression). The temperature contribution is negligible compared to the frequency term. We moreover assume a frequency-independent behavior as a general guess for Drude models. The line fit in Fig. 5(c) assumes the bulk Debye

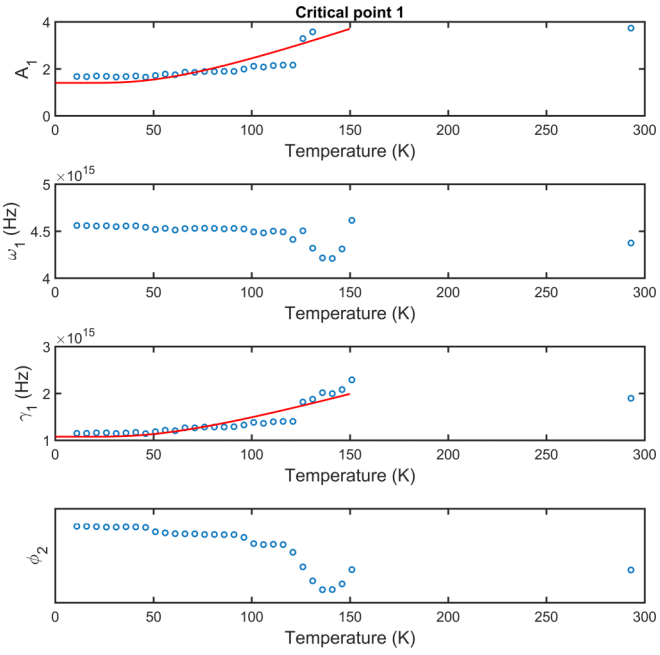

FIG. 6. Critical point 1 parameters A_1, ω_1, γ_1, and ϕ_1 as a function of the temperature. The red line is a fit of the Drude losses with $\gamma_p = \gamma_{ee} + \gamma_{ep}$, where the electron-electron scattering γ_{ee} is assumed constant and the electron-phonon scattering γ_{ep} obeys Eq. (A3).

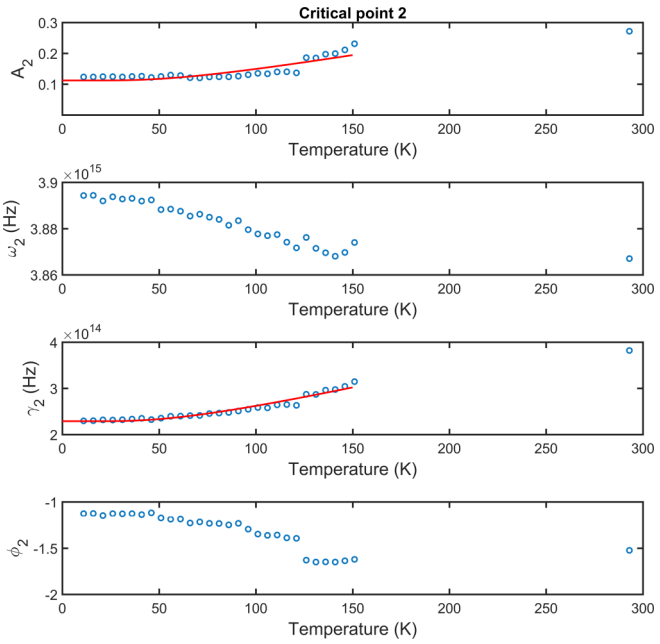

FIG. 7. Critical point 2 parameters A_2, ω_2, γ_2, and ϕ_2 as a function of the temperature. The red lines are fits of oscillator strength A_2 and interband losses γ_2 with Eqs. (A4) and (A5), respectively.

temperature $T_D = 185$ K and qualitatively reproduces the Drude decay behavior up to 150 K. We have considered only the ambient temperature above this value so that it is difficult to discuss the general trend but it seems that the losses does not significantly change above 150 K. We attribute this to the grain boundaries that would govern the losses in the metal above the Debye temperature. Discussion of the role of surface roughness and grain boundaries in the optical losses as a function of the temperature is out of the scope of this work but could benefit from the extended work accomplished to describe the temperature dependence of metal resistivity (see, e.g., Ref. [34]).

The two critical points describe the metal behavior close to interband transitions. The first point dominates at angular frequency $\omega_1 \approx 4.5 \times 10^{15}$ rad/s (corresponding to a wavelength $\lambda \approx 420$ nm), whereas the second point dominates at angular frequency $\omega_2 \approx 3.9 \times 10^{15}$ rad/s (corresponding to a wavelength $\lambda \approx 480$ nm). The corresponding oscillator strength $A(T)$, frequency, and damping rate are shown in Figs. 6 and 7 as a function of temperature. We again observe an important variation (about 65%) from cryogenic to ambient temperatures with a jump close to 125 K. These behaviors qualitatively obey the following standard phenomenological model [33]:

$$A_i = A_{i0} + \alpha_i \coth \frac{T_D}{2T}, \tag{A4}$$

$$\gamma_i = \gamma_{i0} + g_i \coth \frac{T_D}{2T}. \tag{A5}$$

[1] M. Moskovits, Surface-enhanced spectroscopy, Rev. Mod. Phys. **57**, 783 (1985).

[2] H. A. Atwater and A. Polman, Plasmonics for improved photovoltaic devices, Nat. Mater. **9**, 205 (2010).

[3] J. Homola, Surface plasmon resonance sensors for detection of chemical and biological species, Chem. Rev. **108**, 462 (2008).

[4] R. Gordon, D. Sinton, K. L. Kavanagh, and A. G. Brolo, A new generation of sensors based on extraordinary optical transmission, Acc. Chem. Res. **41**, 1049 (2008).

[5] S. E. Lee and L. P. Lee, Biomolecular plasmonics for quantitative biology and nanomedicine, Curr. Opin. Biotechnol. **21**, 489 (2010).

[6] A. V. Akimov, A. Mukherjee, C. L. Yu, D. E. Chang, A. S. Zibrov, P. R. Hemmer, H. Park, and M. D. Lukin, Generation of single optical plasmons in metallic nanowires coupled to quantum dots, Nature (London) **450**, 402 (2007).

[7] A. G. Curto, G. Volpe, T. H. Taminiau, M. P. Kreuzer, R. Quidant, and N. F. van Hulst, Unidirectional emission of a quantum dot coupled to a nanoantenna, Science **329**, 930 (2010).

[8] V. Giannini, A. I. Fernández-Domínguez, S. C. Heck, and S. A. Maier, Plasmonic nanoantennas: Fundamentals and their use in controlling the radiative properties of nanoemitters, Chem. Rev. **111**, 3888 (2011).

[9] A. F. Koenderink, On the use of Purcell factors for plasmon antennas, Opt. Lett. **35**, 4208 (2010).

[10] B. Lee, I.-M. Lee, S. Kim, D.-H. Oh, and L. Hesselink, Review on subwavelength confinement of light with plasmonics, J. Mod. Opt. **57**, 1479 (2010).

[11] M. Kuttge, E. J. R. Vesseur, J. Verhoeven, H. J. Lezec, H. A. Atwater, and A. Polman, Loss mechanisms of surface plasmon polaritons on gold probed by cathodoluminescence imaging spectroscopy, Appl. Phys. Lett. **93**, 113110 (2008).

[12] E. M. Schmidlin and H. J. Simon, Observation of long range surface plasmon decay length by optical second harmonic generation, Appl. Opt. **28**, 3323 (1989).

[13] H. Raether, *Surface Plasmons on Smooth and Rough Surfaces and on Gratings* (Springer, Berlin, 1988).

[14] M. Mayy, G. Zhu, E. Mayy, A. Webb, and M. A. Noginov, Low temperature studies of surface plasmon polaritons in silver films, J. Appl. Phys. **111**, 094103 (2012).

[15] S. V. Jayanti, J. H. Park, A. Dejneka, D. Chvostova, K. M. McPeak, X. Chen, S.-H. Oh, and D. J. Norris, Low-temperature enhancement of plasmonic performance in silver films, Opt. Mater. Express **5**, 1147 (2015).

[16] M. Liu, M. Pelton, and P. Guyot-Sionnest, Reduced damping of surface plasmons at low temperatures, Phys. Rev. B **79**, 035418 (2009).

[17] B. Ji, E. Giovanelli, B. Habert, P. Spinicelli, M. Nasilowski, X. Xu, N. Lequeux, J.-P. Hugonin, F. Marquier, J.-J. Greffet, and B. Dubertret, Non-blinking quantum dot with a plasmonic nanoshell resonator, Nat. Nanotechnol. **10**, 170 (2015).

[18] C. Lethiec, J. Laverdant, H. Vallon, C. Javaux, B. Dubertret, J.-M. Frigerio, C. Schwob, L. Coolen, and A. Maître, Measurement of Three-Dimensional Dipole Orientation of a Single Fluorescent Nanoemitter by Emission Polarization Analysis, Phys. Rev. X **4**, 021037 (2014).

[19] P. B. Johnson and R. W. Christy, Optical constants of the noble metals, Phys. Rev. B **6**, 4370 (1972).

[20] K. M. McPeak, S. V. Jayanti, S. J. Kress, S. Meyer, S. Iotti, A. Rossinelli, and D. J. Norris, Plasmonic films can easily be better: Rules and recipes, ACS Photonics **2**, 326 (2015).

[21] S. K. Ozdemir, Temperature effects on surface plasmon resonance: Design considerations for an optical temperature sensor, J. Lightwave Technol. **21**, 805 (2003).

[22] P. Etchegoin, E. L. Ru, and M. Meyer, An analytic model for the optical properties of gold, J. Chem. Phys. **125**, 164705 (2006).

[23] J. Leng, J. Opsal, H. Chu, M. Senkoa, and D. E. Aspnes, Analytic representations of the dielectric functions of materials for device and structural modeling, Thin Solid Films **313**, 132 (1998).

[24] A. Vial and T. Laroche, Comparison of gold and silver dispersion laws suitable for FDTD simulations, Appl. Phys. B **93**, 139 (2008).

[25] R. R. Chance, A. Prock, and R. Silbey, Molecular fluorescence and energy transfer near interfaces, Adv. Chem. Phys. **37**, 65 (1978).

[26] G. Colas des Francs, J. Barthes, A. Bouhelier, J. C. Weeber, A. Dereux, A. Cuche, and C. Girard, Plasmonic Purcell factor and coupling efficiency to surface plasmons. Implications for addressing and controlling optical nanosources, J. Opt. **18**, 094005 (2016).

[27] D. Canneson, I. Mallek-Zouari, S. Buil, X. Quélin, C. Javaux, B. Mahler, B. Dubertret, and J.-P. Hermier, Strong Purcell effect in single thick shell CdSe/CdS nanocrystals coupled to localized surface plasmons, Phys. Rev. B **84**, 245423 (2011).

[28] D. Canneson, I. Mallek-Zouari, S. Buil, X. Quélin, C. Javaux, B. Dubertret, and J.-P. Hermier, Enhancing the fluorescence of individual thick shell CdSe/CdS nanocrystals by coupling to gold structures, New J. Phys. **14**, 063035 (2012).

[29] C. Javaux, B. Mahler, B. Dubertret, A. Shabaev, A. V. Rodina, A. L. Efros, D. R. Yakovlev, F. Liu, M. Bayer, G. Camps, L. Biadala, S. Buil, X. Quélin, and J.-P. Hermier, Thermal activation of non-radiative Auger recombination in charged colloidal nanocrystals, Nat. Nanotechnol. **8**, 206 (2013).

[30] D. Canneson, L. Biadala, S. Buil, X. Quélin, C. Javaux, B. Dubertret, and J.-P. Hermier, Blinking suppression and biexcitonic emission in thick-shell CdSe/CdS nanocrystals at cryogenic temperature, Phys. Rev. B **89**, 035303 (2014).

[31] Y.-S. Park, A. V. Malko, J. Vela, Y. Chen, Y. Ghosh, F. García-Santamariá, J. A. Hollingsworth, V. I. Klimov, and H. Htoon, Near-Unity Quantum Yields of Biexciton Emission from CdSe/CdS Nanocrystals Measured Using Single-Particle Spectroscopy, Phys. Rev. Lett. **106**, 187401 (2011).

[32] M. Saba, M. Aresti, F. Quochi, M. Marceddu, M. A. Loi, J. Huang, D. V. Talapin, A. Mura, and G. Bongiovanni, Light-induced charged and trap states in colloidal nanocrystals detected by variable pulse rate photoluminescence spectroscopy, ACS Nano **7**, 229 (2013).

[33] H. Reddy, U. Guler, A. Kildishev, A. Boltasseva, and V. Shalaev, Temperature-dependent optical properties of gold thin films, Opt. Mater. Express **6**, 2776 (2016).

[34] R. Munoz and C. Arenas, Size effects and charge transport in metals: Quantum theory of the resistivity of nanometric metallic structures arising from electron scattering by grain boundaries and by rough surfaces, Appl. Phys. Rev. **4**, 011102 (2017).